Electronic Supplementary Information (ESI)

Lattice disordering influencing on photocarrier dynamics in lead halide perovskites

Haijuan Zhang, [a] Taiyang Zhang, [b] Yong Wang, [b] Yuetian Chen, [b] Yixin Zhao,*[b] and Jie Chen*[a]

[a]Center for Ultrafast Science and Technology, Key Laboratory for Laser Plasmas (Ministry of Education), School of Physics and Astronomy, Collaborative Innovation Center of IFSA (CICIFSA), Shanghai Jiao Tong University

800 Dongchuan Road, Shanghai 200240 (P. R. China)

[b]School of Environmental Science and Engineering, Shanghai Jiao Tong University, 800 Dongchuan Road, Shanghai 200240 (P. R. China)

Corresponding authors: yixin.zhao@sjtu.edu.cn; jiec@sjtu.edu.cn

S1. Sample preparation and static state characterization

The room temperature x-ray diffraction patterns of β-$CsPbI_3$, γ-$CsPbI_3$, β-$MAPbI_3$ and β-$FA_{0.9}Cs_{0.1}PbI_3$ films are presented in Figure S1 (a). The main diffraction peaks are sharp and the signals of the impurities such as PbI_2 or δ phase do not appear, indicating that all samples are well crystallized with a pure single phase. Their morphologies were determined by scanning electron microscope (Figure S1 (c)), which show that all have a grain size varying from 200 to 800 nm and a compact surface without observable pinholes. The high quality of the samples confirmed by the above characteristic measurements supplies us an objective environment for further exploration of their dynamic carrier properties by pump-probe ultrafast transient reflectance (TR) measurements. Their bandgaps were determined by the absorption spectra shown in Figure S1 (b). The absorption edges of the β-$CsPbI_3$, γ-$CsPbI_3$, β-$MAPbI_3$ and β-$FA_{0.9}Cs_{0.1}PbI_3$ films appear at 738, 716, 786 and 802 nm, corresponding to the bandgaps of 1.68, 1.73, 1.58 and 1.55 eV, respectively. The near-edge 790 nm (1.57 eV) was chosen as the probe for a high transient sensitivity. The far above-edge 395 nm (3.14 eV) was chosen as the pump due to its high absorption coefficient of all samples, about 1.5×10^5 cm^{-1} and therefore with a designed sample thickness of 200 nm, the majority, 99.9%, of the pumping photons will be absorbed by the samples. For all the samples, a sapphire (Al_2O_3 polycrystalline, diameter Ø=25.4 mm) disk was applied as the substrate, and its insulating nature enables us to isolate the intrinsic dynamics of perovskites from any process in or with the substrate.

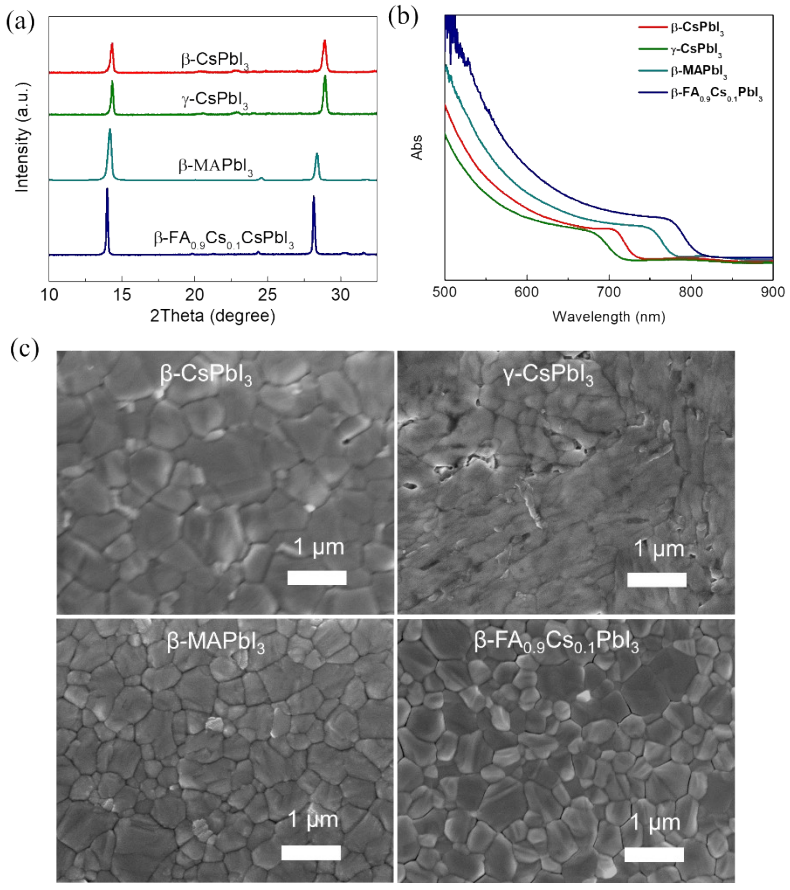

Fig. S1. (a) X-ray diffraction patterns, (b) absorption spectra and (c) scanning electron microscope images of β-$CsPbI_3$, γ-$CsPbI_3$, β-$MAPbI_3$ and β-$FA_{0.9}Cs_{0.1}PbI_3$ films.

S2. Transient reflectance measurements and kinetics for β-$MAPbI_3$, γ-$MAPbI_3$ and β-$FA_{0.9}Cs_{0.1}PbI_3$ films

The Transient reflectance (TR) measurements were carried out with a 1 kHz Ti:sapphire laser system (Legend Elite HE+USP-III, Coherent, Inc.), delivering 40 fs pulses at a center wavelength of 790 nm (1.57 eV). The laser was split into two beams, with one at the fundamental frequency acting as the probe, and the other converted into 395 nm by a Type I BBO acting as the pump. A larger pump spot (~5 mm) and a much smaller probe spot (0.6 mm) were employed to realize easily a spatial overlap between them. The pump fluence was varied from 2 to 41 μJ/cm^2, much lower than the damage threshold of the samples, whereas the probe fluence was fixed at ~0.1 μJ/cm^2. TR signal was obtained by varying the time difference between the pump and probe pulses with a high-precision delay stage located in the pump optical path. During the data acquisition, the pump beam was modulated into 220 Hz by an optical chopper and the induced intensity changes of the reflected probe beam were collected by the lock-in amplification technique.

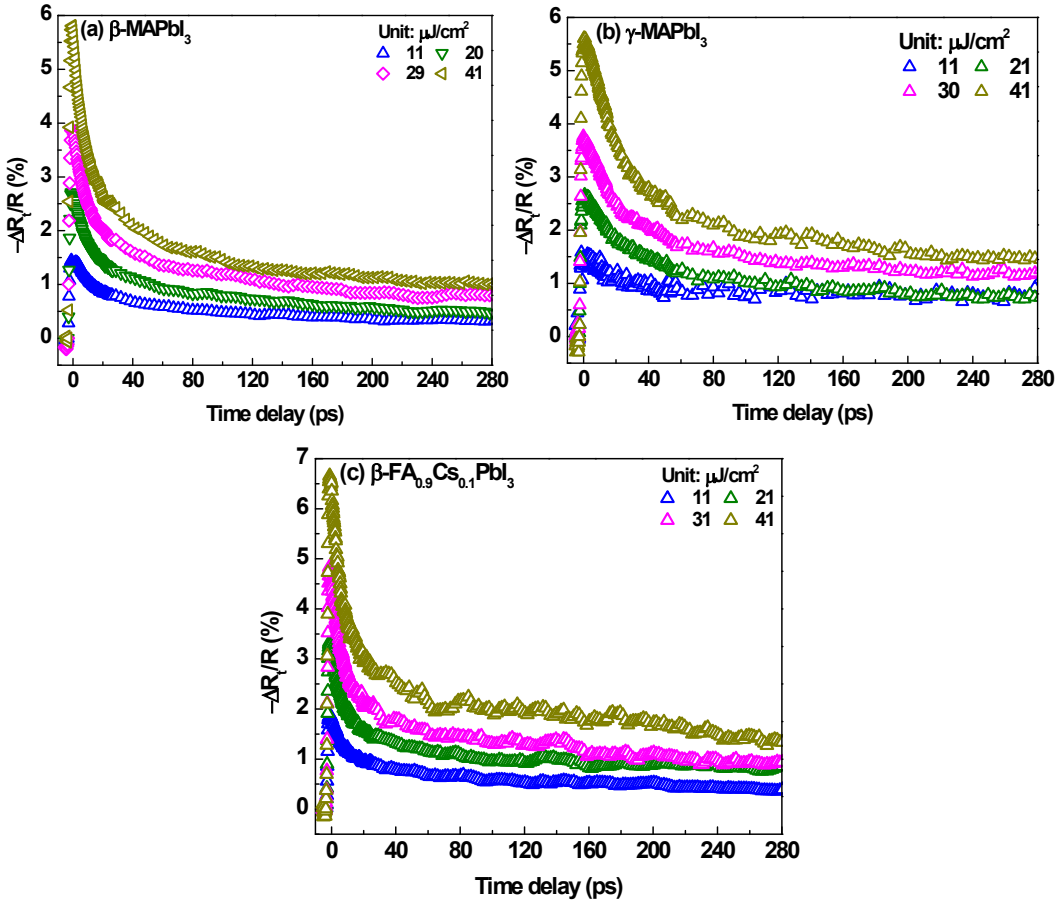

Fig. S2. Pump fluence dependent TR kinetics for (a) β-$MAPbI_3$, (b) γ-$MAPbI_3$ and (c) β-$FA_{0.9}Cs_{0.1}PbI_3$ films.

S3. Analysis of carrier dynamics dominated by the first and second order mechanisms

As shown in Fig. 1 (c) of the main text, the maximum relative transient reflectance change $\left(-\frac{\Delta R_t}{R}\right)_{max}$ linearly depends on the initial excited carrier density n_0, described as $\left(-\frac{\Delta R_t}{R}\right)_{max} = bn_0$. The linear coefficient b is fit to be 5.4×10^{-21} cm^3 for β-$CsPbI_3$ and β-$FA_{0.9}Cs_{0.1}PbI_3$, 4.8×10^{-21} cm^3 for β-$MAPbI_3$, 4.5×10^{-21} cm^3 for γ-$MAPbI_3$ and 4.1×10^{-21} cm^3 for γ-$CsPbI_3$. The transient photocarrier density n_t is therefore obtained by the real time reflectivity change $\frac{\Delta R_t}{R}$ as scribed as $-\frac{\Delta R_t}{R} = bn_t$.

As discussed in the main text, the photocarrier depopulation process in perovskites is usually described by a simple rate equation [1]

$$-\frac{dn_t}{dt} = k_1 n_t + k_2 {n_t}^2 + k_3 {n_t}^3 \quad (1)$$

Three terms on the right hand side can be successively ascribed to: (1) a first-order Shockley-Reed (trap state-mediated) recombination or carrier diffusion out of the probing region; (2) a second-order non-geminate/free carrier recombination; and (3) a three-body Auger recombination, with k_1, k_2 and k_3 being the corresponding depopulation rate constants, respectively. Because of the very low pump fluence applied in this study, the third order process was neglected.

We first quickly examined the experimental data by assuming the recovery process is dominated by either the first or the second term. If the recovery process is dominated by the first-order mechanism, equation (1) can be simplified to $-\frac{dn_t}{dt} = k_1 n$ and therefore $n_t = n_1 e^{-k_1 t}$. Similarly, $n_t = \frac{n_2}{k_2 n_2 t + 1}$ if it is dominated by the second-order mechanism. Here n_1 and n_2 are the photocarrier densities depopulated through the first-order and the second-order mechanisms, respectively. Thus, if the recovery process is dominated by the first-order mechanism, the associated reflectivity change follows $-\frac{\Delta R_t}{R} = bn_1 e^{-k_1 t}$ or $ln\left(-\frac{\Delta R_t}{R}\right) = \ln(bn_1) - k_1 t$, i. e. $ln\left(-\frac{\Delta R_t}{R}\right)$ should depend linearly on time delay *t*.

Similarly, if the recovery process is dominated by the second-order mechanism, the

reflectivity change satisfies $-\frac{\Delta R_t}{R} = b\frac{n_2}{k_2 n_2 t + 1}$ or $\left(-\frac{\Delta R_t}{R}\right)^{-1} = \frac{k_2}{b}t + \frac{1}{bn_2}$, i.e. $\left(-\frac{\Delta R_t}{R}\right)^{-1}$ should depend linearly on t. The time dependent $ln\left(-\frac{\Delta R_t}{R}\right)$ and $\left(-\frac{\Delta R_t}{R}\right)^{-1}$ for all five samples are summarized in Figures S3 and S4, respectively. We found that the photocarrier depopulation of all samples is dominated by a first-order process in the initial tens of picoseconds, and then by a second-order process which lasts up to several hundreds of picoseconds. As a result, next we analyzed the data more accurately by considering both the first and second terms of equation (1) as detailed in the main text.

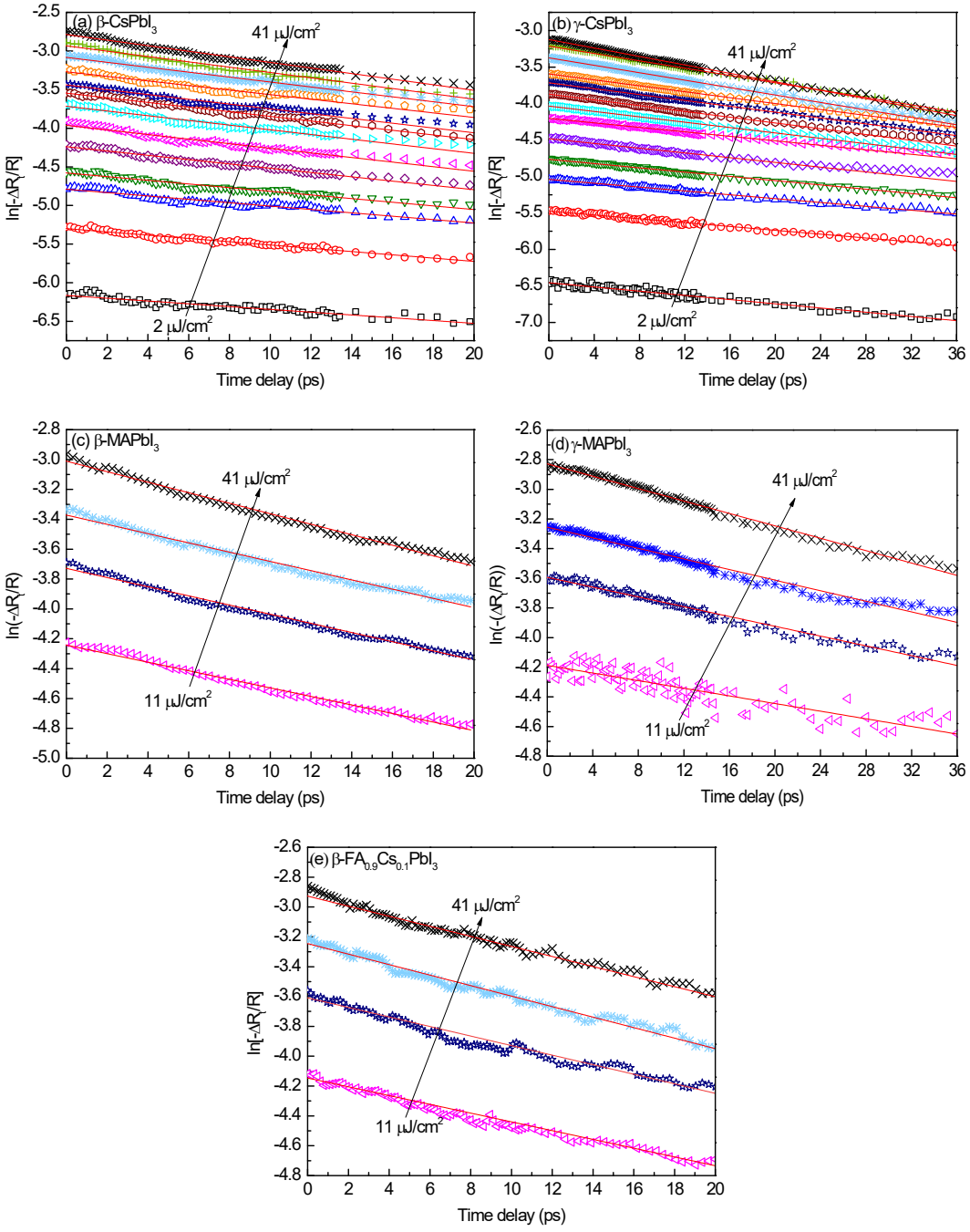

Fig. S3. Time dependences of $\ln(-\frac{\Delta R_t}{R})$ during the recovery process for (a) β-$CsPbI_3$, (b) γ-$CsPbI_3$, (c) β-$MAPbI_3$, (d) γ-$MAPbI_3$ and (e) β-$FA_{0.9}Cs_{0.1}PbI_3$. The solid lines are the fitting to the experimental data presented as scattered points. The arrows indicate the rise in pump fluence.

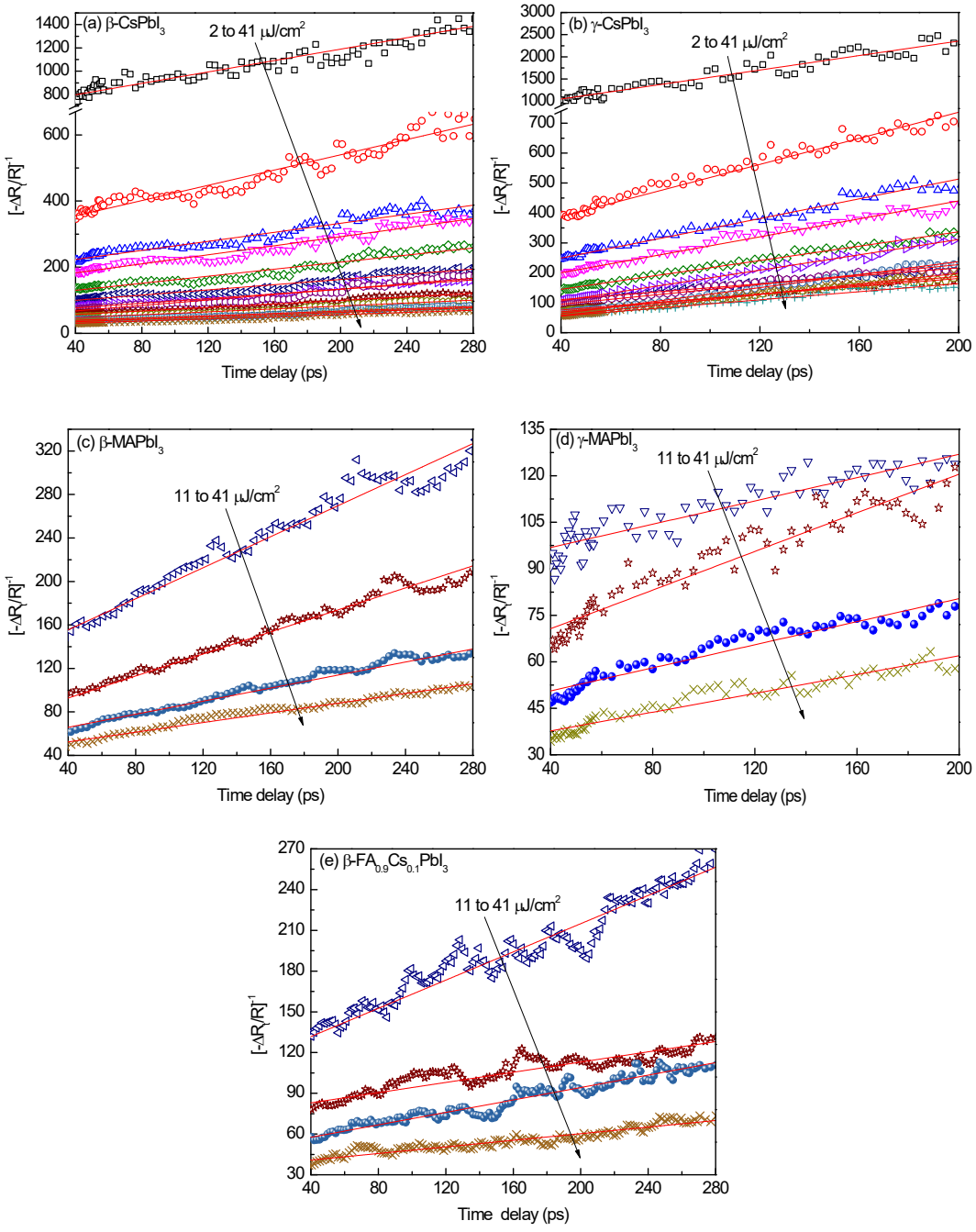

Fig. S4. Time dependences of $(-\frac{\Delta R_t}{R})^{-1}$ during the recovery process for (a) β-$CsPbI_3$, (b) γ-$CsPbI_3$, (c) β-$MAPbI_3$, (d) γ-$MAPbI_3$ and (e) β-$FA_{0.9}Cs_{0.1}PbI_3$. The solid lines are the fitting to the experimental data presented as scattered points. The arrows indicate the rise in pump fluence.

References

1. J. S. Manser and P. V. Kamat, *Nat. Photonics*, 2014, **8**, 737-743.